Exchange and polarization effect in high-order harmonic imaging of molecular structures

Sukiasyan, Suren; Patchkovskii, Serguei; Smirnova, Olga; Brabec, Thomas; Ivanov, Misha Yu

Publisher's version / Version de l'éditeur:
https://doi.org/10.1103/PhysRevA.82.043414
Physical Review A, 82, 4, pp. 043414/1-043414/12, 2010-10-15

Exchange and polarization effect in high-order harmonic imaging of molecular structures

Suren Sukiasyan,[1,*] Serguei Patchkovskii,[2] Olga Smirnova,[3] Thomas Brabec,[4] and Misha Yu. Ivanov[1]

[1]*Department of Physics, Imperial College London, South Kensington Campus, SW7 2AZ London, United Kingdom*

[2]*National Research Council, 100 Sussex Drive, Ottawa, Ontario K1A 0R6, Canada*

[3]*Max-Born Institute for Nonlinear Optics and Short Pulse Spectroscopy, Max-Born-Strasse 2A, D-12489 Berlin, Germany*

[4]*Physics Department and Center for Research in Photonics, University of Ottawa, 150 Louis Pasteur, Ottawa, Ontario K1N 6N5, Canada*

(Received 30 June 2010; published 15 October 2010)

We analyze the importance of exchange, polarization, and electron-electron correlation in high-order harmonic generation in molecules interacting with intense laser fields. We find that electron exchange can become particularly important for harmonic emission associated with intermediate excitations in the molecular ion. In particular, for orbitals associated with two-hole one-particle excitations, exchange effects can eliminate structure-related minima and maxima in the harmonic spectra. Laser-induced polarization of the neutral molecule may also have major effects on orbital structure-related minima and maxima in the harmonic spectra. Finally, we show how exchange terms in recombination can be viewed as a shakedownlike process induced by sudden electronic excitation in the ion.

DOI: 10.1103/PhysRevA.82.043414 PACS number(s): 33.80.Rv, 32.80.Rm

I. INTRODUCTION

High-order harmonic generation (HHG) by molecules interacting with intense laser fields is a unique process that records information about molecular structure and dynamics, potentially with subfemtosecond temporal and subangstrom spatial resolution [1]. Intense experimental and theoretical efforts are currently aimed at realizing this potential.

Applications of HHG spectroscopy to dynamic imaging typically rely on the so-called three-step model [2]. Within this physical picture, an electron (i) is liberated from the molecular (or atomic) orbital, (ii) is accelerated by an intense laser field, and (iii) emits a harmonic photon upon returning to the parent ion and recombining to the initial bound state of the neutral molecule. Recombination of the returning continuum electron is described by the matrix element $\langle\psi_b|\hat{r}|\chi_c\rangle$. Here ψ_b is the bound part of the wave function (usually the initial, ground, state ψ_g), and the continuum wave function χ_c is usually written in the single-active-electron (SAE) approximation. In the simplest case of $\psi_b \approx \psi_g$, the matrix element encodes structural information about the ground-state wave function ψ_g [1].

Accounting for nuclear motion shows that HHG spectra also record information about nuclear dynamics between ionization and recombination (see, e.g., [1,3,4]). Additional opportunities for imaging arise in pump-probe-type experiments, with HHG used as a probe of nuclear dynamics induced by an ultrashort pump (see, e.g., [5,6]). The pump-probe setup in harmonic generation can also be used to follow electronic rearrangements induced by the underlying nuclear dynamics at conical intersections [7].

While the SAE picture typically associated with the simplest version of the three-step model can be satisfactory for atoms (particularly noble gasses), in molecules multielectron effects start to play a significantly more prominent role already at the level of what is commonly referred to as "exchange terms" in recombination (see, e.g., [8–10]). Radiative recombination exhibits the richness and complexity of its counterpart, the one-photon ionization. Not surprisingly, harmonic emission reflects this complexity (see, e.g., [11–14]), for example, through the coupling of different recombination channels via electron-electron interaction. Channel coupling induced by the returning electron can play an important role in significantly increasing the efficiency of harmonic generation at frequencies $\sim 10^2$ eV [14].

The participation of multiple ionic states not only during recombination, but also at all steps of the harmonic generation process [6,12,15–19], introduces additional opportunities for dynamic imaging. For example, it opens a route to following attosecond dynamics of holes between ionization and recombination [15–18]. However, the drawback is the need for accurate theoretical description of strong-field dynamics, starting with strong-field ionization, for both single [20–28] and multiple ionization channels [29–31]. Quantitative modeling of harmonic generation requires one to consider not only multiple ionization and recombination channels corresponding to different states of the molecular ion, but also their coupling during strong-field ionization and between ionization and recombination [13,15,32].

Thus, from the theoretical perspective, the simplicity of the three-step model hides a rich variety of effects demanding adequate theoretical description. These include: (i) (multielectron) polarization of the bound wave function in the neutral molecule and in the ion by the laser field [13,33,34], (ii) laser-induced electronic excitations on the subcycle time scale [32,33,35,36], including excitations in the ion between ionization and recombination, (iii) correlation-induced virtual and real excitations of the ionic electrons by the returning continuum electron, immediately prior and during recombination [13,14,37], (iv) excitations of collective modes (such as plasmons) in highly polarizable molecules and clusters [38,39], by both the laser field and the recolliding electron.

Therefore, qualitative and quantitative understanding of various multielectron effects, such as exchange and correlation between the continuum and the bound electrons, in the presence of a strong laser field is paramount for using HHG as a spectroscopic tool for dynamic imaging.

*s.sukiasyan@imperial.ac.uk

The photorecombination step in harmonic generation is often thought of as the inverse of photoionization. In photoionization, the importance of electron exchange and virtual and real excitations induced by the correlation between the outgoing continuum electron and the electrons of the core is well known. Thus, it is by no means surprising that similar effects are important during photorecombination. Quantitative theoretical analysis of several such effects in a model molecular system is the focus of this article.

Specifically, we focus on the interplay of polarization, recollision-induced excitations in the ion, and exchangelike contributions during the photorecombination step of HHG. Our approach allows us to include both the strong laser field and the electron-electron interaction on an equal footing.

We also discuss the physical process that underlies exchangelike contributions to recombination. We show that these contributions describe a shakedown-type process, which can be viewed as follows. First, the dipole operator induces an electronic transition in the ion, changing its state from, say, n to m. This excitation changes the interaction between the ion and the continuum electron and hence the structure of the correlated continuum. Consequently, the continuum wave packet describing the recolliding electron in channel n finds itself in channel m, where it acquires a bound component. More specifically, it has substantial overlap with the Dyson orbital corresponding to channel m (the Dyson orbital is the overlap of the ground state of the neutral molecule with the ionic state $|m\rangle$). This overlap is nothing but the amplitude of recombination of the continuum electron, forced by the sudden change of the continuum.

The rest of the article is organized as follows. In Sec. II we give a qualitative discussion of the photorecombination step in HHG vs one-photon ionization in photoelectron spectroscopy. Section III describes the general approach and computational details. Section IV introduces the main tool of our analysis: ionic eigenstate resolved (IER) expansion of the multidimensional wave function. Section V discusses our results. Section VI concludes the article.

II. PHOTOIONIZATION VS PHOTORECOMBINATION IN HIGH HARMONIC GENERATION

In the time domain, quantum expressions for high harmonic radiation can be written as a product of three amplitudes: ionization, continuum propagation, and recombination [40]. This general structure is maintained in the frequency domain, with the important caveat that one has to sum over the contribution of several trajectories that correspond to the same energy of the returning electron (see, e.g., [41]). Since (i) at first glance the photo-recombination step looks like the inverse of photoionization and (ii) one-photon ionization is a well-studied process equipped with sophisticated theoretical tools, it is tempting to complex-conjugate accurate photoionization matrix elements $\langle\chi_c|\hat{r}|\psi_g\rangle$ and use them for the recombination step of the HHG process. This is the key component of the so-called "quantitative rescattering theory" [11], compared to the standard approaches based on the strong-field approximation. The same suggestion is at the core of the analytical expressions proposed in Ref. [14]. We note that the same concept was originally developed and used in [42] for the quantitative description of the recollision dynamics and correlated double ionization.

Such an approach is a significant improvement compared to the SAE theory with a plane-wave continuum. However, the recombination matrix elements are calculated for the *laser field-free* scattering problem. One should be cautious when using the field-free cross sections for a strong-field process. In principle, the laser field present during recombination can affect both the scattering states of the continuum electron and the bound states of the molecular ion, as well as modify the coupling between different recombination channels.

Field-free scattering states are solutions of the *stationary* scattering problem. In the language of electron trajectories, these states include both small and large-angle scattering events, as well as complex multiple scattering, which, from the time-domain perspective, evolves over a longer time and should be particularly sensitive to the strong external laser field present during the interaction. Note that in typical HHG experiments the strong driving laser field changes from zero to several volts per angstrom in a quarter cycle, that is, in about 0.65 fs for near-infrared radiation at $\lambda = 800$ nm. Thus, the scattering problem is far from stationary for complex scattering events.

A particular property of HHG is its selectivity to specific classes of "quantum trajectories" [43–45]. These "trajectories" arise as a result of using the saddle point method for calculating multidimensional integrals in the quantum description of HHG. An alternative language developed by Kuchiev and Ostrovsky [41,46,47], which describes HHG in terms of multiple channels, leads to the same physical picture once the saddle point method is applied [41]. The language of quantum trajectories has been used extensively and successfully for analyzing various aspects of strong-field dynamics, including the properties of harmonic generation and other recollision-driven physical processes (see, e.g., [48–60]). Particularly important in harmonic generation are the so-called "short" trajectories, which correspond to the simplest electron motion in the continuum with the shortest time delay between ionization and recombination. Phase-matching of high harmonic emission in the macroscopic medium [61] typically favors these trajectories while suppressing the contribution of longer and more complex trajectories (see, e.g., review [43] or the pioneering articles [44,45,62]; see also [63] for the role of phase-matching in generating single attosecond pulses). Thus, the contribution of continuum resonances (e.g., shape resonances) and complex scattering trajectories to the recombination cross sections will be vulnerable not only to the strong external field, but also to the phase matching in the macroscopic response measured in the experiments.

For simple short trajectories that experience single scattering on the ionic core, Ref. [64] showed when and how the effect of the laser field can be simplified, reducing the recombination matrix element in the strong laser field to the effectively field-free one. We stress, however, that the same conclusion does not apply to multiple scattering and complex trajectories that stay in the vicinity of the core for a time comparable to a quarter of the laser cycle.

Finally, recombination in HHG involves a continuum wave packet produced by strong-field ionization. The shape of this wave packet does not always correspond to the asymptotic

plane wave front at infinity, typically used in the stationary scattering problem. Coherent preparation of the continuum state $|\chi_c\rangle$ in the recombination matrix element $\langle\psi_g|\hat{r}|\chi_c\rangle$ is another important difference from the conventional, time-independent scattering theory.

Consider, for example, experiments with aligned molecules, which are typical for a HHG setup. Strong-field ionization from a molecular orbital with nodal planes, for example, ionization from the highest occupied molecular orbital (HOMO) in O_2 or CO_2 along or perpendicular to the molecular axis, will not only be suppressed, but it will also produce a continuum wave packet with a nodal plane along the direction of propagation. Such nodal plane in the returning wave packet will affect its density near the ionic core during the recombination step of the harmonic generation. It will also change the symmetry of the populated continuum states and the recombination matrix element.

This discussion outlines physical aspects that one has to keep in mind developing quantitative theoretical description of HHG. It shows why such description remains challenging decades after the discovery of HHG. The fundamental difficulty is the need to address intense field multielectron dynamics, keeping both the laser field and the electron-ion interaction on equal footing. The solution of the time-dependent multielectron Schrödinger equation is beyond reach [65–67]. Approximate methods, such as the time-dependent Hartree-Fock (HF) [68], frozen-core (FC) [69], and time-dependent density functional theory [70], neglect all or part of electron correlation; their accuracy is not controlled. Even if the Schrödinger equation is solved, extracting the underlying physics from the multidimensional wave function is a formidable problem in its own right.

We solve the time-dependent Schrödinger equation for a two-electron model diatomic molecule with two spatial dimensions per electron. The numerical study uses the multiconfiguration time-dependent Hartree (MCTDH) method (see review [71] and references therein), in which Hartree orbitals form a time-dependent basis set for the expansion of the properly antisymmetrized two-electron wave function. Optimization of the multiconfiguration expansion brings the computational costs down to a level comparable with conventional one-electron calculations and opens the door to a systematic analysis of multielectron effects in HHG. For the analysis of the role of exchange and multielectron correlation effects in HHG we use an IER expansion of the multidimensional wave function [13]. This technique allows us to quantify the physical mechanisms and the role of various multielectron effects.

III. GENERAL APPROACH

We solve the time-dependent Schrödinger equation for a model diatomic molecule containing two electrons, each in two dimensions (2D). The system Hamiltonian is

$$H = \sum_{i=1}^{2}[\hat{T}_i + \mathbf{r}_i \cdot \mathbf{E} + V(\mathbf{r}_i)] + V_{ee}(\mathbf{r}_1,\mathbf{r}_2), \tag{1}$$

where index i labels the electrons, $\mathbf{r} = (x,y)$ is the 2D space vector, and $\hat{T}$ is the kinetic-energy operator. Interaction with the laser field $\mathbf{E}(t)$ is described in the dipole approximation and length gauge. The laser field is polarized along the x axis, which also coincides with the alignment of the molecular axis. The nuclei are positioned at $(\pm R/2,0)$, and their potential is

$$V(\mathbf{r}) = -1/\sqrt{(x \pm R/2)^2 + y^2 + a_{ne}^2}. \tag{2}$$

The two-electron interaction in Eq. (1) is given by

$$V_{ee} = 1/\sqrt{(\mathbf{r}_2 - \mathbf{r}_1)^2 + a_{ee}^2}. \tag{3}$$

Here a_{ne} and a_{ee} are the Coulomb softening parameters. They are chosen to set the ionization potential of our model molecule, I_p, to the ionization potential of a N_2 molecule $I_p = 15.58$ eV at the N_2 equilibrium internuclear distance $R = 2.08$ bohrs, yielding $a_{ne} = a_{ee} = 0.64$. The two-electron binding energy in this case is 46.8 eV. The nuclei are held fixed during the propagation.

For our numerical analysis we employ the multiconfiguration time-dependent Hartree (MCTDH) method (see [71] and references therein). MCTDH uses the expansion of the wave function in variationally optimized lower-dimensional time-dependent basis functions,

$$\Psi(\mathbf{X}_1,\ldots,\mathbf{X}_m,t) = \sum_{j_1=1}^{n_1}\cdots\sum_{j_m=1}^{n_m} A_{j_1,\ldots,j_m}(t)\prod_{\kappa=1}^{m}\varphi_{j_\kappa}^{(\kappa)}(\mathbf{X}_\kappa,t), \tag{4}$$

where $\mathbf{X}_1,\ldots,\mathbf{X}_m$ are one- or multidimensional coordinates, representing *m single particles*, in which the multidimensional system is split, $A_J(t)$ are the time-dependent expansion coefficients ($J \equiv j_1,\ldots,j_m$), and the $\varphi_{j_\kappa}^{(\kappa)}(\mathbf{X}_\kappa,t)$ represent the time-dependent expansion functions (orbitals) for single-particle κ (see [71] Secs. 3.1 and 4.5). Computational efficiency of the MCTDH method stems from the time dependence of single-particle basis functions (orbitals), which adapt to dynamics "on the fly" and hence describe it better than time-independent functions. Hence, the desired accuracy is achieved with fewer orbitals. Increasing the number n_κ of expansion orbitals converges the MCTDH wave function (4) toward the exact one.

The equations of motion for $A_J(t)$ and $\varphi_j^{(\kappa)}(\mathbf{X}_\kappa,t)$ are derived from the Dirac-Frenkel variational principle [72,73] (see [71] Secs. 2.2 and 3.1):

$$\langle\delta\Psi|H - i\partial_t|\Psi\rangle = 0. \tag{5}$$

The time-dependent form of both the expansion coefficients and the single-particle functions requires one to impose additional constraints to ensure their uniqueness. One such constraint is the orthonormality of the single-particle functions, $\varphi_j^{(\kappa)}(t)$,

$$\langle\varphi_j^{(\kappa)}(0)|\varphi_l^{(\kappa)}(0)\rangle = \delta_{jl}, \tag{6}$$

which can be preserved during time propagation using the constraints

$$\langle\varphi_j^{(\kappa)}(t)|\dot{\varphi}_l^{(\kappa)}(t)\rangle = -i\langle\varphi_j^{(\kappa)}(t)|g^{(\kappa)}|\varphi_l^{(\kappa)}(t)\rangle, \tag{7}$$

where $g^{(\kappa)}$ is an arbitrary Hermitian operator acting exclusively on the single-particle κ (see Ref. [71], Secs. 3.1–3.3).

Coupled equations of motion for the coefficients and the single-particle orbitals can be written as (here for the simplicity we set $g^{(\kappa)} = 0$ for all single particles) (see Ref. [71], Sec. 3.2)

$$i\dot{A}_J = \sum_L \langle \Phi_J | H | \Phi_L \rangle A_L \tag{8}$$

$$i\dot{\varphi}^{(\kappa)} = (1 - P^{(\kappa)})(\rho^{(\kappa)})^{-1} \langle \mathbf{H} \rangle^{(\kappa)} \varphi^{(\kappa)}, \tag{9}$$

where

$$\Phi_J = \prod_{\kappa=1}^{m} \varphi_{j_\kappa}^{(\kappa)} \tag{10}$$

and

$$\varphi^{(\kappa)} = \left(\varphi_1^{(\kappa)}, \ldots, \varphi_{n_\kappa}^{(\kappa)}\right)^T. \tag{11}$$

$P^{(\kappa)}$ is the projector on the space spanned by the basis functions for the single-particle κ,

$$P^{(\kappa)} = \sum_{j=1}^{n_\kappa} \left|\varphi_j^{(\kappa)}\right\rangle\left\langle\varphi_j^{(\kappa)}\right|, \tag{12}$$

$\langle \mathbf{H} \rangle^{(\kappa)}$ and $\rho^{(\kappa)}$ are the mean-field and density matrices, respectively, with corresponding elements

$$\langle H \rangle_{jl}^{(\kappa)} = \left\langle \Psi_j^{(\kappa)} \middle| H \middle| \Psi_l^{(\kappa)} \right\rangle, \tag{13}$$

$$\rho_{jl}^{(\kappa)} = \left\langle \Psi_j^{(\kappa)} \middle| \Psi_l^{(\kappa)} \right\rangle. \tag{14}$$

In these definitions $\Psi_l^{(\kappa)}$'s are the so-called single-hole functions,

$$\Psi_l^{(\kappa)} = \sum_J^{\kappa} A_{J_l^\kappa} \varphi_{j_1}^{(1)} \cdots \varphi_{j_{\kappa-1}}^{(\kappa-1)} \varphi_{j_{\kappa+1}}^{(\kappa+1)} \cdots \varphi_{j_m}^{(m)}. \tag{15}$$

where the sum does not include the single-particle κ and $J_l^\kappa = j_1, \ldots, j_{\kappa-1} l j_{\kappa+1}, \ldots, j_m$.

Since the Hamiltonian in our problem does not contain spin-mixing operators, the initial spin state is conserved and for two electrons can be easily factored out. Therefore, we only need to deal with the spatial part of the wave function. Our initial state is singlet (ground state), leading to the symmetric spatial part. Symmetry of the spatial part of the wave function is preserved during the propagation.

In contrast with the conventional Hartree or Hartree-Fock (HF) methods, a MCTDH single-particle is a mathematical object that does not necessarily represent a real particle. The choice of the MCTDH single particles is rather a matter of numerical efficiency in the integration of the MCTDH equations of motions in Eqs. (8) and (9), and is usually dictated by the total number of dimensions, dynamics of the system, and the form of the Hamiltonian. This choice influences the efficiency of the method significantly.

For our system with a total of four spatial degrees of freedom, we find that it is computationally efficient to choose one-dimensional expansion orbitals, $\varphi_j(x,t)$. An alternative choice for the MCTDH single particles is to correspond to real particles (electron). This would also be the case for the multiconfiguration time-dependent Hartree-Fock (MCTDHF) approach [74]. Given that we explicitly antisymmetrize our total wave function, with this latter choice of single-particle orbitals the two approaches would be identical. The latter choice of single-particle orbitals, which forces one to deal with higher-dimensional expansion functions and hence higher-dimensional coupled time-dependent Schroedinger equations, increases the overall computational cost.

For our total 4D wave function Ψ the MCTDH expansion yields

$$\Psi(x_1,y_1;x_2,y_2,t) = \sum_{j_1=1}^{n_1} \cdots \sum_{j_4=1}^{n_4} A_{j_1 j_2 j_3 j_4}(t) \varphi_{j_1}^{(1)}(x_1,t) \times \varphi_{j_2}^{(2)}(y_1,t) \varphi_{j_3}^{(3)}(x_2,t) \varphi_{j_4}^{(4)}(y_2,t). \tag{16}$$

Here n_i for $i = 1, \ldots, 4$ denotes the number of expansion functions along the coordinates (x_1, y_1, x_2, y_2) respectively. The Cartesian coordinates (x_1, y_1) and (x_2, y_2) characterize the positions of the first and the second electrons, $\mathbf{r}_1 = (x_1, y_1)$ and $\mathbf{r}_2 = (x_2, y_2)$, respectively.

The choice of one-dimensional single-particle orbitals as our basis brings computational benefits only if one can effectively deal with the multidimensional integrals that describe the interaction of real physical particles. To solve this problem, the Hamiltonian must be represented with the same type of expansion as the system wave function, that is, as a sum of products of 1D potentials. For the nuclear potential, $V(\mathbf{r})$, this can be done easily using expansion in the basis of natural potentials [see [71,75] (Sec. 6.1)]: $V(\mathbf{r}) = \sum_i v_i(x) u_i(y)$. High accuracy of expansion is achieved typically with several terms.

The most critical issue is treatment of electron-electron interaction, V_{ee} in Eq. (3), which couples all four degrees of freedom. The same expansion in natural potentials for V_{ee} yields two-dimensional potentials:

$$V_{ee}(x_1,y_1;x_2,y_2) = \sum_i v_i(x_1 - x_2) u_i(y_1 - y_2). \tag{17}$$

We avoid further expansion of $v_i(x_1 - x_2)$ and $u_i(y_1 - y_2)$ natural potentials in 1D potential basis since it requires too many terms. Instead, we efficiently calculate matrix elements of the potentials $v_i(x_1 - x_2)$ and $u_i(y_1 - y_2)$ using the fact that these 2D potentials depend on the differences $x_1 - x_2$ and $y_1 - y_2$ only. Therefore, calculation of integrals can be done using the convolution theorem combined with fast Fourier transform. For example, for $v_i(x_1 - x_2)$ we have to deal with matrix elements

$$\left\langle \varphi_{j_1}^{(1)}(x_1) \varphi_{j_2}^{(2)}(x_2) \middle| v_i(x_1 - x_2) \middle| \varphi_{l_1}^{(1)}(x_1) \varphi_{l_2}^{(2)}(x_2) \right\rangle, \tag{18}$$

where $\varphi_j^{(\kappa)}(x)$'s are the time-dependent basis functions. The treatment of the two-dimensional integral as a convolution allows one to replace its calculation with two Fourier transforms, where the fast Fourier transform can be utilized. The final numerical cost is proportional to $4N\log N$, instead of N^2, where N is the number of grid points. The numerical cost is further lowered by employing the so-called *constant mean-field* integration scheme, where the mean fields and density matrices in Eq. (9), as well as the Hamiltonian matrix in Eq. (8), are calculated at larger time intervals and are kept constant in between [see [71,76] (Chapter 5)].

The ground state of the system, which determines the initial condition for the time-dependent problem, is found by imaginary time propagation of the properly symmetrized initial condition [71,77]. Unless mentioned otherwise, atomic units (a.u.)

are used. A spatial grid spacing of 0.4 a.u. is found to be sufficient to obtain converged results. The laser field is linearly polarized along the direction of the nuclear axis, $\mathbf{E}(t) = \mathbf{E_0} \sin^2(\pi t/T)\cos(\omega t)$, with a peak intensity of 10^{14} W/cm^2 and a wavelength of 800 nm. A laser pulse includes 10 cycles "base-to-base"; that is, the total duration is set to $T = 26$ fs.

In each coordinate, we add complex absorbing potentials of the form $W(x) = -i\eta(|x| - x_c)^3$ for $|x| \geqslant x_c$ and $\eta = 0.0005$ to the system Hamiltonian. Their aim is to absorb the "multiple return" trajectories and partially absorb the so-called "long" trajectories while keeping short trajectories intact. This approach allows us to approximate spectra for HHG in gases in typical experimental conditions, in which focusing of the laser pulse and the positioning of the gas jet favors short trajectories [43] via phase matching. For our laser parameters, we use $x_c = 18$. Moving the onset of the absorbing boundary further out to leave all trajectories intact has virtually no influence on the key multielectron effects observed in our HHG calculations. Due to absorption the propagated wave function is not exact anymore. We use the term *total* for this wave function and all results obtained using it.

An important aspect of absorbing the "far-away" part of the continuum wave function is its impact on convergence. Indeed, on the one hand, a very large number of expansion functions is required to describe detailed interference patterns in the total wave function at very large distances from the core. On the other hand, these patterns give no contribution the high-order harmonic emission. Absorption of the distant continuum part of wave function naturally reduces the complexity of the total wave function and thus reduces the total number of expansion functions, n_i, in Eq. (16) required to reach convergence. The numerical efficiency improves crucially, since computational cost scales exponentially with n_i. Using 15 basis functions per degree of freedom ($n_1 = n_2 = n_3 = n_4 = 15$), we assure a convergence of the total wave function with accuracy better than 10^{-7}. A single propagation takes only several hours on a single-core CPU. In contrast, calculation of converged correlated two-electron spectra, angle and energy-resolved, required more than 25 functions per degree of freedom [78].

IV. IONIC EIGENSTATE RESOLVED APPROACH

To analyze the role of multielectron dynamics, we use the ionic eigenstate resolved (IER) expansion of the wave function [13]. First, we solve full time-dependent Schrödinger equation to find multielectron wave function. Then, we expand this wave function over a basis of bound electronic eigenstates of the ion, $\psi(\mathbf{r}_2)$, indentifying $\mathbf{r}_2$ as the "bound" ionic electron. This expansion allows one to identify different harmonic generation channels [13,15], that is, different participating ionic states and hence different orbitals and different electronic configurations participating in the process.

Had the expansion basis over $\mathbf{r}_2$ been complete, such expansion would have been exact, and the bound $\mathbf{r}_2$ electron would have been also found in the continuum states, while the correlated functions of the $\mathbf{r}_1$ electron would have automatically included bound ionic states. However, in our expansion we only include several bound ionic states, restricting the basis set. Therefore, the expanded wave function is approximate and must be additionally antisymmetrized with respect to the bound $\mathbf{r}_2$ and continuum $\mathbf{r}_1$ electrons.

For the singlet initial state, the spatial part of the IER wave function should have the symmetric form

$$\Psi_M(\mathbf{r}_1,\mathbf{r}_2,t) = \sum_{k=1}^{M} [\chi_k(\mathbf{r}_1,t)\psi_k(\mathbf{r}_2) + \psi_k(\mathbf{r}_1)\chi_k(\mathbf{r}_2,t)]. \quad (19)$$

Here Ψ_M is the IER wave function, M is the number of bound ionic eigenstates included in the expansion. The time-dependent wave packets $\chi_k(\mathbf{r},t)$ are correlated to the ionic eigenstates $\psi_k(\mathbf{r})$. These wave packets may include not only continuum, but also excited electronic (e.g., Rydberg) states.

To extract the wave packets χ_k from the total wave function $\Psi(\mathbf{r}_1,\mathbf{r}_2,t)$, we introduce projections $\phi_k(\mathbf{r}_1)$ of the total wave function $\Psi(\mathbf{r}_1,\mathbf{r}_2,t)$ onto the ionic eigenstates, $\psi_k(\mathbf{r}_2)$,

$$\phi_k(\mathbf{r}_1,t) = \langle\psi_k(\mathbf{r}_2)|\Psi(\mathbf{r}_1,\mathbf{r}_2,t)\rangle. \quad (20)$$

Substituting the ansatz Eq. (19) into Eq. (20), we obtain a set of integral equations for $\chi_k(\mathbf{r}_1,t)$:

$$\chi_k(\mathbf{r}_1,t) = \phi_k(\mathbf{r}_1,t) - \sum_{j=1}^{M} \langle\psi_k(\mathbf{r}_2)|\chi_j(\mathbf{r}_2,t)\rangle\psi_j(\mathbf{r}_1,t). \quad (21)$$

One of the solutions of these integral equations is

$$\chi_k(\mathbf{r}_1,t) = \left[1 - \frac{1}{2}\sum_{j=1}^{M} |\psi_j(\mathbf{r}_1)\rangle\langle\psi_j(\mathbf{r}_1)|\right]\phi_k(\mathbf{r}_1,t). \quad (22)$$

The physical meaning of this result is as follows. If we were doing our expansion in a natural way, that is, by approximating $\chi_k \approx \phi_k = \langle\psi_k|\Psi\rangle$, we would have obtained

$$\Psi_M(\mathbf{r}_1,\mathbf{r}_2,t) \approx \sum_{k=1}^{M} [\phi_k(\mathbf{r}_1,t)\psi_k(\mathbf{r}_2) + \psi_k(\mathbf{r}_1)\phi_k(\mathbf{r}_2,t)]. \quad (23)$$

Since the wave packets ϕ_k can overlap with ionic eigenfunctions ψ_j, the terms $\langle\psi_j|\phi_k\rangle\psi_k\psi_j$ with $j = 1,\ldots,M$ are counted twice. Therefore, we apply the projector

$$\hat{P} = 1 - \frac{1}{2}\sum_{j=1}^{M} |\psi_j(\mathbf{r})\rangle\langle\psi_j(\mathbf{r})| \quad (24)$$

to remove the double-counted contributions. In the limit of $M \to \infty$ Ψ_M converges to the exact wave function, excluding the part describing the double ionization. The IER wave function Ψ_M is invariant to the choice of the initial phase of ionic eigenstates ψ_i.

The Ψ_M describes the cumulative content of the first M ionic eigenstates in the total wave function. For $M = 1$, Ψ_M describes the part of the total wave function, where one electron remains in the ionic ground state. Within our approach, it is the closest possible wave function to the SAE approximation. However, both exchange and electron-electron correlation are still present in the wave function $\Psi_{M=1}$, since $\chi_{k=1}$ is obtained from the exact wave function and therefore includes the effect of coupling to all excited states during and after ionization. For the same reason, $\Psi_{M=1}$ goes beyond the HF ansatz.

Since we employ absorbing potentials in our propagation, the harmonic spectra are calculated using the expectation

value of the acceleration operator. For the harmonic spectrum including first M ionic eigenstates we obtain

$$\mathbf{I}_M(\Omega) = \left| \int \langle \Psi_M | \hat{\mathbf{a}}_1 + \hat{\mathbf{a}}_2 | \Psi_M \rangle e^{i\Omega t} dt \right|^2, \tag{25}$$

where $\hat{\mathbf{a}}_{1,2}$ is the acceleration operator of corresponding first and second electron. Taking into account electron exchange symmetry, Eq. (25) can be rewritten as

$$\mathbf{I}_M(\Omega) = 4 \left| \int \langle \Psi_M | \hat{\mathbf{a}}_{\mathbf{r}_1} | \Psi_M \rangle e^{i\Omega t} dt \right|^2, \tag{26}$$

where $\hat{\mathbf{a}}_{\mathbf{r}_1}$ is the acceleration operator excluding the electron-electron interaction, which can be expressed as [79]

$$\hat{\mathbf{a}}_{\mathbf{r}_1} = -\frac{\partial V}{\partial \mathbf{r}_1} - \mathbf{E}(t). \tag{27}$$

Here V is the potential of the nuclei and $\mathbf{E}(t)$ is the laser electric field. For molecules aligned parallel or perpendicular to the polarization vector of the linearly polarized laser pulse we can substitute $\hat{\mathbf{a}}_{\mathbf{r}_1}$ with

$$\hat{a}_{x_1} = -\frac{\partial V}{\partial x_1} - E(t) \tag{28}$$

and we denote the corresponding spectrum $I_M(\Omega)$. For arbitrary alignment angle, $I_M(\Omega)$ corresponds to measuring only the component of harmonic emission with polarization parallel to that of the laser field.

To isolate the role of electronic polarization induced by the laser field in the neutral molecule, we also calculate the approximate spectrum:

$$I_M^G(\Omega) = 4 \left| \int \alpha(t) \langle \Psi_g | \hat{a}_{x_1} | \Psi_M \rangle e^{i\Omega t} dt \right|^2. \tag{29}$$

Here Ψ_g is the two-electron ground state and $\alpha(t) = \langle \Psi(t) | \Psi_g \rangle$. The IER ansatz Ψ_M, especially for lower M, describes well the part of the wave function with one electron bound and one in the continuum. Thus, it is well suited for analyzing harmonics with photon energies above I_p created via free-bound transitions, that is, above the 11th harmonic order in our case. Finally, replacing Ψ_M with Ψ in Eqs. (26) and (29) yields the total spectrum, $I(\Omega)$ and $I^G(\Omega)$, respectively.

V. RESULTS AND DISCUSSION

A. Role of polarization in the HHG

Comparison of total harmonic yields, $I(\Omega)$ and $I^G(\Omega)$, demonstrates the role of polarization of the neutral molecule in harmonic emission. For our model molecule, this difference can be found in Figs. 1(a) and 1(b). A comparison shows that neglecting laser-induced electronic polarization of the neutral molecule can yield order-of-magnitude difference (see also [80]). For high harmonics, the signal strengths are rather close—but with one important qualitative difference: including polarization of the neutral molecule [panel (b)] suppresses the minimum in the harmonic spectrum near H19–H23. The minimum, described in [68], is associated with the structure of the molecular orbitals and results from

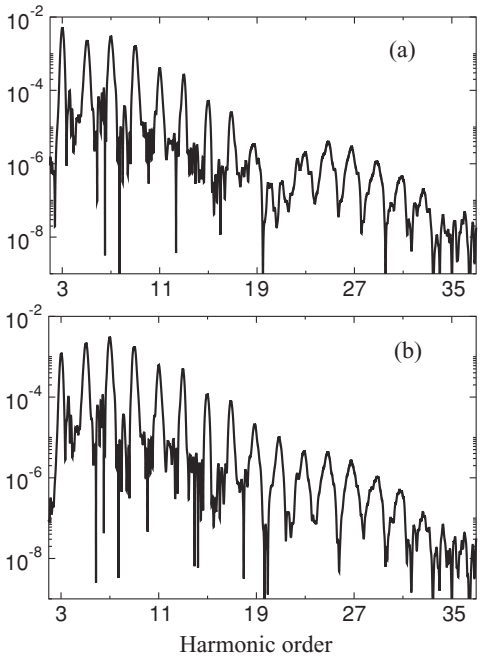

FIG. 1. Total harmonic yields, I and I^G, calculated by (a) Eq. (29) and (b) Eq. (26), with total wave function Ψ instead of Ψ_M.

the destructive two-center interference in the recombination to the two atoms of the diatomic molecule. The fact that destructive interference is more pronounced for the field-free final state is clear: Polarization displaces electron density in the neutral molecule toward one of the nuclei, breaking perfect spatial symmetry of the ground state and making destructive interference incomplete.

The formal analysis is as follows. The polarized ground state of the neutral molecule can be written as $\Psi_g(t) = \sum_m \langle \Phi_m | \Psi_g(t) \rangle \Phi_m$, where Φ_m's are the field-free two-electron bound states. Recombination into the polarized state can therefore be schematically represented as an interplay of recombination into different field-free channels. These channels will have different minima and maxima structure: As noted in [81] (for one-electron systems), the interference minimum for even-symmetry (gerade) final states turns into the interference maximum for odd-symmetry (ungerade) states. The interplay of different channels will therefore smooth the structural minimum associated with the two-center interference in the recombination to the field-free ground state.

In the limit of large internuclear distances, the effect of laser field on the bound electron can become even more dramatic due to the field-induced electron localization in the neutral, molecule which may completely alter positions of destructive and constructive interference [33].

B. Role of exchange symmetry

Our model system represents a type of tightly bound two-electron system. The binding energies of the first four ionic eigenstates are −31 eV, −20.4 eV, −15 eV, and −10.9 eV, respectively. The ionic eigenstates are shown in Fig. 2. Taking into account these four ionic state channels in Eq. (26) describes the harmonic yield almost exactly. Including the

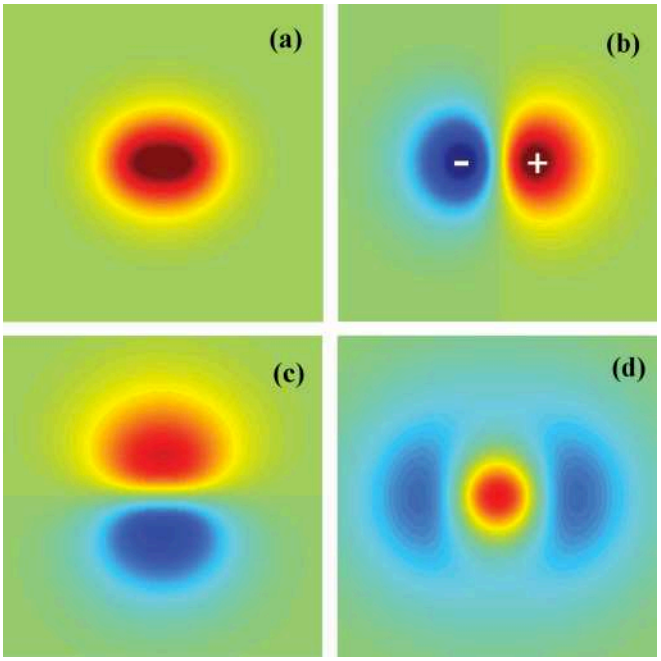

FIG. 2. (Color online) Wave functions for the first four ionic bound states of our model system. The corresponding energies are (a) −31 eV, (b) −20.4 eV, (c) −15 eV, and (d) −10.9 eV, respectively. The color coding shows the sign of the wave function, red for positive and blue for negative.

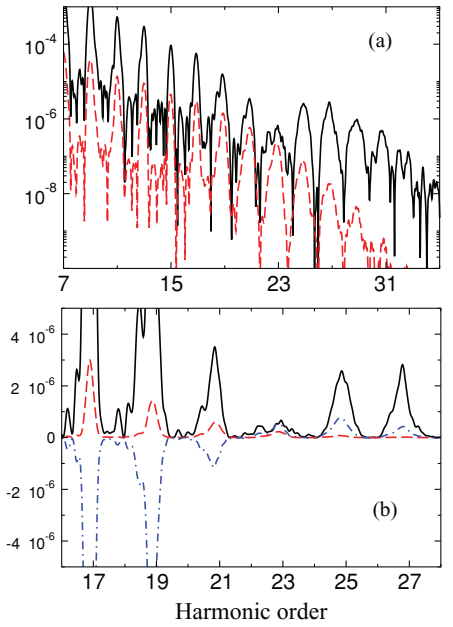

FIG. 3. (Color online) Harmonic spectrum of direct and exchange channels associated with the ground ionic state. Panel (a) shows direct (solid black line) and exchange (dashed red line) harmonic yields, in panel (b) the interference part between two channels is added (blue dot-dashed line) on the linear scale.

first two ionic states already yields 80%–90% accuracy in the harmonic spectra. The third eigenstate has almost negligible contribution for molecules aligned parallel to the laser field polarization due to its symmetry [13]. Thus, our study is focused on the ionic ground and the first excited states and the role of exchange symmetry and exchange terms for each corresponding channel.

We note that terms usually referred to as exchange in recombination (see, e.g., [8–10]) appear already for purely Hartree-type wave function, since the total dipole operator includes the sum of all single-particle dipoles. This is also the reason why exchange terms have been referred to as "cradle" in [29], but here we keep the usual terminology.

1. Ground-state channel

The IER wave function for the ionic ground-state channel is [see Eq. (23)]

$$\Psi_1(\mathbf{r}_1,\mathbf{r}_2,t) = \chi_1(\mathbf{r}_1,t)\psi_1(\mathbf{r}_2) + \chi_1(\mathbf{r}_2,t)\psi_1(\mathbf{r}_1) \quad (30)$$

or, using the definition of χ_1,

$$\Psi_1(\mathbf{r}_1,\mathbf{r}_2,t) = \phi_1(\mathbf{r}_1,t)\psi_1(\mathbf{r}_2) + \psi_1(\mathbf{r}_1)\phi_1(\mathbf{r}_2,t) - \langle\psi_1(\mathbf{r}_1)|\phi_1(\mathbf{r}_1,t)\rangle\psi_1(\mathbf{r}_1)\psi_1(\mathbf{r}_2). \quad (31)$$

For the analysis of direct versus exchange contribution, we exclude the polarization of the ground state of the neutral molecule; that is, we use Eq. (29) for harmonic yield. Then the matrix elements for the direct and exchange contributions are

$$M^{(1)}_{\rm dir}(t) = \alpha(t)\langle\Psi_g(\mathbf{r}_1,\mathbf{r}_2)|\hat{a}_{x_1}|\psi_1(\mathbf{r}_2)\phi_1(\mathbf{r}_1,t)\rangle, \quad (32)$$

$$M^{(1)}_{\rm ex}(t) = \alpha(t)\langle\Psi_g(\mathbf{r}_1,\mathbf{r}_2)|\hat{a}_{x_1}|\psi_1(\mathbf{r}_1)\phi_1(\mathbf{r}_2,t)\rangle. \quad (33)$$

The total harmonic intensity associated with the ionic ground state includes the sum of direct and exchange terms and their interference. Even when the exchange term is small compared to the direct contribution, the interference term is significant.

Figure 3(a) shows two separate harmonic yields, corresponding to the direct and the exchange contributions associated with the ionic ground-state channel. The contributions are calculated using the matrix elements in Eqs. (32) and (33). The direct contribution exceeds the exchange contribution by between half and two orders of magnitude. As expected, the direct contribution shows an interference minimum. However, such a minimum is absent in the exchange channel. This result is general: It is related to different spatial symmetries of the direct and exchange contributions, as discussed in what follows.

Interference of direct and exchange terms is shown in Fig. 3(b). First, the interference term is significant. Its amplitude varies between 20% and 100% (in the vicinity of the structural minimum) of the direct emission amplitude. Second, the destructive interference of direct and exchange contributions before the structural minimum (in the direct yield) turns into constructive interference after the structural minimum. Taking into account that the phase of the direct contribution changes by π while passing the structural minimum [68], we infer that the interference has a generally destructive character.

This result is related to the opposite spatial symmetry of the direct and exchange matrix elements [Eqs. (32) and (33)] discussed in what follows. Let us expand the ground state of the neutral molecule in the basis of ionic states,

$$\Psi_g(\mathbf{r}_1,\mathbf{r}_2) = \sum_{i=1}^{n} \psi_i^{\mathrm{D}}(\mathbf{r}_1)\psi_i(\mathbf{r}_2). \tag{34}$$

Here

$$\psi_i^{\mathrm{D}}(\mathbf{r}_1) = \langle \psi_i(\mathbf{r}_2)|\Psi_g(\mathbf{r}_1,\mathbf{r}_2)\rangle \tag{35}$$

are the Dyson orbitals for the ground state of the neutral molecule. Note that our two-electron wave function is normalized to unity, and thus we do not need the factor $\sqrt{N} = \sqrt{2}$ for the definition of the Dyson orbitals ($N = 2$ is the number of electrons). For the first four states of the ion in our model system ($n = 4$), their norms are $\|\psi_i^{\mathrm{D}}\|^2 = 0.94, 0.027, 0.004, 0.022$, for $i = 1,2,3,4$. With these four states, Ψ_g is reproduced with 99.4% accuracy.

We now note the following two properties of the ground state $\Psi_g(\mathbf{r}_1,\mathbf{r}_2)$. First, it has gerade symmetry, $\Psi_g(\mathbf{r}_1,\mathbf{r}_2) = \Psi_g(-\mathbf{r}_1,-\mathbf{r}_2)$. Therefore, the gerade symmetry of the ionic ground state $\psi_1(\mathbf{r}_1)$ dictates that $\psi_1^{\mathrm{D}}(\mathbf{r}_2)$ is also gerade. Ungerade symmetry of $\psi_2(\mathbf{r}_1)$ dictates that $\psi_2^{\mathrm{D}}(\mathbf{r}_2)$ is also ungerade.

Second, electron-electron repulsion dictates that the electron density is higher when $\mathbf{r}_1 = -\mathbf{r}_2$, as compared to $\mathbf{r}_1 = \mathbf{r}_2$. Given gerade symmetry of the first term in the sum Eq. (34), it falls upon the second term to reduce the electron density when both electrons are on the same side of the nuclei. Therefore, for $\psi_2(-x_2,y_2) < 0$ and $\psi_2(x_2,y_2) > 0$ (where x_2 is positive and y_2 is arbitrary), we obtain that $\psi_2^{\mathrm{D}}(-x_1,y_1) > 0$ and $\psi_2^{\mathrm{D}}(x_1,y_1) < 0$ (x_1 is positive, y_1 is arbitrary). That is, the phase of the wave function for first excited ionic state and the phase of the corresponding Dyson orbital ψ_2^{D} are flipped, as seen by comparing Fig. 4(b) with Fig. 2(b).

We can use the expansion Eq. (34) to analyze the interplay of direct and exchange terms. For analytical analysis we use length rather than acceleration gauge, where the analysis of arising integrals is much simpler. Substituting Eq. (34) into Eq. (32) for the direct contribution and into Eq. (33) for the exchange contribution, we find

$$M_{\mathrm{dir}}^{(1)}(t) = \alpha(t)\langle \psi_1^{\mathrm{D}}(\mathbf{r}_1)|\hat{x}_1|\phi_1(\mathbf{r}_1,t)\rangle, \tag{36}$$

$$M_{\mathrm{ex}}^{(1)}(t) = \alpha(t)\sum_{i=1}^{4}\langle \psi_i^{\mathrm{D}}(\mathbf{r}_1)|\phi_1(\mathbf{r}_1,t)\rangle\langle\psi_i(\mathbf{r}_2)|\hat{x}_2|\psi_1(\mathbf{r}_2)\rangle. \tag{37}$$

The physics behind the exchange contribution is as follows: The dipole operator induces transition *in the ion* from the state ψ_1 to a state $\psi_{i>1}$, and the returning electron recombines into the hole described by the corresponding Dyson orbital ψ_i^{D}. In our case, only the term $i = 2$ contributes to the exchange part.

The additional symmetry property imposed by electron-electron repulsion, which requires that if $\psi_2(-x_2,y_2) < 0$ then $\psi_2^{\mathrm{D}}(-x_1,y_1) > 0$ (for positive x_1 and x_2), is responsible for opposite signs of the direct and exchange contributions before the structural minimum. For the given orbital shapes, shown in Fig. 2, the transition matrix element in the ion $\langle\psi_2(\mathbf{r}_2)|x_2|\psi_1(\mathbf{r}_2)\rangle$ is positive and the functions $\psi_2^{\mathrm{D}}(\mathbf{r}_1)$ and $\psi_1^{\mathrm{D}}(\mathbf{r}_1)\times x_1$ have opposite signs. Hence, the phases of direct and exchange terms are shifted by π, and their interference reduces direct contribution.

The norms of the Dyson orbitals are crucial in defining the magnitudes of the direct and exchange harmonic yields. Since $\|\psi_1^{\mathrm{D}}\|^2 \gg \|\psi_2^{\mathrm{D}}\|^2$, direct contribution dominates for the ground-state channel, see Fig. 3(a). However, the situation is quite different for the excited ionic state.

2. *Excited-state channel*

The key role of excited states in HHG has now been recognized theoretically and experimentally. There is, however, an important qualitative aspect of HHG channels associated with excited ionic states in our system. Indeed, our system has only two electrons and hence only a single initially occupied orbital in the HF picture. Therefore, population of excited ionic states cannot be viewed as a removal of an electron from a deeper orbital. In our case, excited states of the ion correspond to two-hole one-particle configurations. Therefore, direct one-photon recombination is suppressed: Removal of a two-hole excitation with a single dipole operator requires help from an electron-electron correlation. In what follows, we see that exchange terms become particularly important under such circumstances.

The importance of two-hole one-particle configuration is by no means an artifact of our system. Such states are ubiquitous in polyatomic molecules and can even lie below the first ionization threshold. They can be multiphoton excited during the laser pulse before ionization, leading to ions in two-hole one-particle configurations. Depending on the field strength, laser wavelength, and excitation energy in the ion, such states can also be excited by the laser field between ionization and recombination. Finally, they can be excited by the recolliding electron during recombination [13]. Naturally, similar recollision-induced excitations can also contribute to the excited ionic channels associated with single-hole configurations.

Importance of laser-field assisted recollision-induced excitation during recombination has generally been underestimated in HHG. However, our calculations show that it should

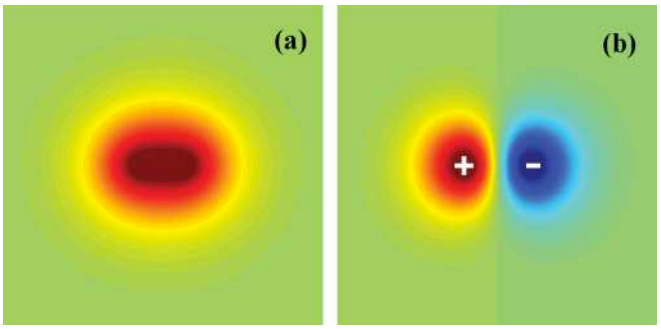

FIG. 4. (Color online) Dyson orbitals ψ_i^{D} for the first two ionic bound states of our model system. (a) $i = 1$, (b) $i = 2$. The color coding shows the sign of the wave function, red for positive and blue for negative.

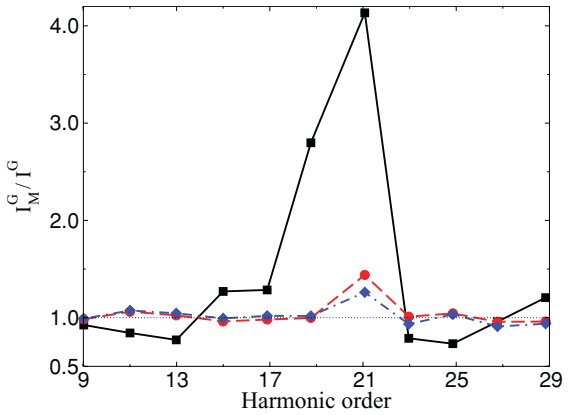

FIG. 5. (Color online) Ratio of the harmonic intensities calculated for a finite number of the ionic channels to the total yield, I_M^G/I^G, for $M = 1$ (black squares), $M = 2$ (red circles), and $M = 4$ (blue diamonds).

not be ignored. Figure 5 shows the ratio of the harmonic spectra (29) calculated with the total wave function and with the wave function Ψ_M for $M = 1,2,4$.

When only the ground ionic state is included in the calculation (squares), in the range of the structural minimum total and approximate results differ by more than a factor of 4. The agreement is better for the rest of the spectrum, with a difference up to 40%. The expansion converges quickly with increasing M. When HHG from the first ionic excited state is added (circles), the agreement is within 20% of the total result. The contribution of ψ_3 is negligible due to symmetry. Adding ψ_4 (diamonds) yields an agreement better than 10% with the total result. The polarization of the ground state of the neutral molecule does not eliminate the contribution of ionic excited states: For I_1/I we have a difference up to factor 2, and for I_2/I we have agreement better than 20% with the total harmonic yield.

This effect is a result of excitations of the parent ion by the recolliding electron [13]. Discussion regarding the dynamics of the ionic excitations will be published separately [82]. The key factor demonstrating that ionic excitations are induced by the recolliding electron and not by the laser field is the unshifted harmonic cutoff. Laser-induced excitation would have added the energy to the system, shifting the cutoff by about 11 eV in our case. The conclusion regarding the origin of the excitation is supported by monitoring the population of excited ionic states while increasing the ellipticity of the driving laser field. The population of the first excited ionic state is a few percent of the ionic ground-state population for linear polarization and quickly drops to zero with increasing ellipticity.

Analysis of exchange contribution for the first excited ionic state is similar to the preceding analysis for the ground-state channel. Using the expansion of the neutral-molecule ground state into the ionic states Eq. (34), we obtain

$$M_{\rm dir}^{(2)}(t) = \alpha(t)\langle\psi_2^{\rm D}(\mathbf{r}_1)|\hat{x}_1|\phi_2(\mathbf{r}_1,t)\rangle, \tag{38}$$

$$M_{\rm ex}^{(2)}(t) = \alpha(t)\sum_{i=1}^{4}\langle\psi_i^{\rm D}(\mathbf{r}_1)|\phi_2(\mathbf{r}_1,t)\rangle\langle\psi_i(\mathbf{r}_2)|\hat{x}_2|\psi_2(\mathbf{r}_2)\rangle. \tag{39}$$

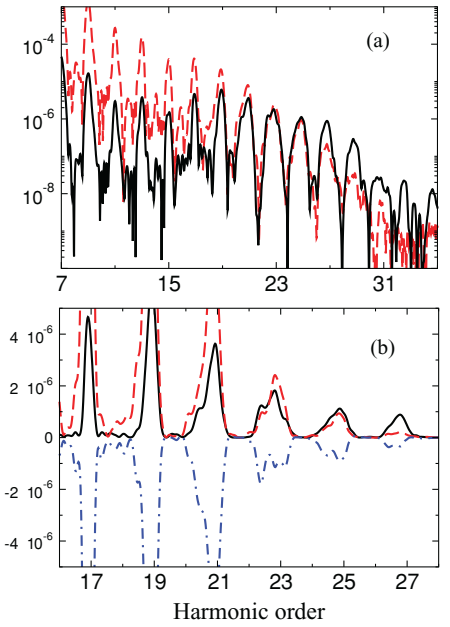

FIG. 6. (Color online) Harmonic spectrum of direct and exchange channels associated with the first excited ionic state. Panel (a) shows direct (solid black line) and exchange (dashed red line) harmonic yields; in panel (b) the interference part between two channels is added (dot-dashed blue line) on the linear scale.

Direct and exchange contributions to the harmonic yield are shown in Fig. 6(a). The structural (two-center interference) maximum appears at harmonic H19 in the direct contribution. Its origin is the ungerade symmetry of the Dyson orbital $\psi_2^{\rm D}$. The behavior of the relative phase of direct and exchange emissions is shown by the interference term plotted in Fig. 6(b). Similar to the ground state, and for the same reasons, the interference between the two terms is destructive. Since passing through the structural maximum does not lead to the phase jump in the direct contribution, the direct-exchange interference remains destructive across the spectrum.

In contrast to the ionic ground-state channel, for the first ionic excited state channel the exchange contribution dominates. Indeed, the direct contribution is now proportional to $\|\psi_2^{\rm D}\|^2$, while the exchange contribution is proportional to $\|\psi_1^{\rm D}\|^2$ [in Eq. (39) the member $i = 1$ clearly dominates]. As a result, the structural maximum is washed out. Thus, exchange contributions may make experimental observation of structural features associated with excited ionic states problematic, at least when it comes to two-hole one-particle configurations, with the correspondingly small norms of the Dyson orbitals for the direct channel.

Destructive interference between the direct and exchange terms makes the situation even more interesting. Indeed, if the direct and exchange contributions are close to each other, their destructive interference can create additional minimum(a) in the total harmonic yield. Position(s) of these new minimum(a) may distort reconstruction of orbital structure [68] or dynamics [15]. Structural minima in the direct contribution to the ground-state channel are one obvious place where other contributions play significant role, and where the destructive interference of the direct and exchange terms from various

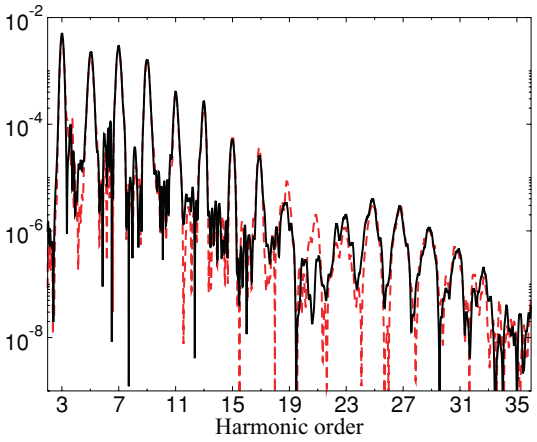

FIG. 7. (Color online) Total harmonic yield I^G (solid black line) and I_1^G (dashed red line). The minima in I_1^G at H19–23 are associated with the structure, while the minimum in I^G at H21 is a result of interference between ionic ground- and excited-state channels.

channels is important. As demonstrated in [83], structural minima in the recombination matrix elements associated with the ground-state channel serve as windows into the other channels, making their contributions more important. The same applies to exchange contributions. An example is seen in Fig. 7, which shows the total harmonic yield. In this figure, the minimum at H23 is associated with the structure. The additional deeper minimum at H21 is induced by the destructive interference between direct and exchange channels associated with ionic ground and excited states.

C. General case

The importance of exchange contribution in HHG spectra has been stressed in [9,37]. Here, we generalize the discussion presented in the previous subsections to the case of a general multielectron system.

Using the same expansion of the multielectron ground state of the neutral molecule into the ionic basis, we find that direct and exchange contributions to the recombination dipole in the channel j can be written as (in the length gauge)

$$\mathbf{M}_{\rm dir}^{(j)}(t) = \alpha(t)\langle\psi_j^{\rm D}(\mathbf{r})|\hat{\mathbf{r}}|\phi_j(\mathbf{r},t)\rangle, \tag{40}$$

$$\mathbf{M}_{\rm ex}^{(j)}(t) = \alpha(t)\sum_i \langle\psi_i^{\rm D}(\mathbf{r})|\phi_j(\mathbf{r},t)\rangle\langle\psi_i|\hat{\mathbf{d}}_{N-1}|\psi_j\rangle. \tag{41}$$

Here the dipole operator $\hat{\mathbf{d}}_{N-1}$ acts on all ionic electrons, and the channel j is associated with an ion in the state ψ_j before the recollision.

Structural features associated with the Dyson orbital of interest $\psi_i^{\rm D}(\mathbf{r})$ are encoded in the direct contribution to the recombination dipole, $\langle\psi_i^{\rm D}(\mathbf{r})|\mathbf{r}|\phi_i(\mathbf{r})\rangle$. However, they can be masked by the structural features of other Dyson orbitals, $\psi_i^{\rm D}(\mathbf{r})$, which are encoded in the exchange contributions. Interference of the direct and exchange terms adds further complexity.

As an example, consider the N_2 molecule aligned perpendicular to the laser polarization. The two channels dominating

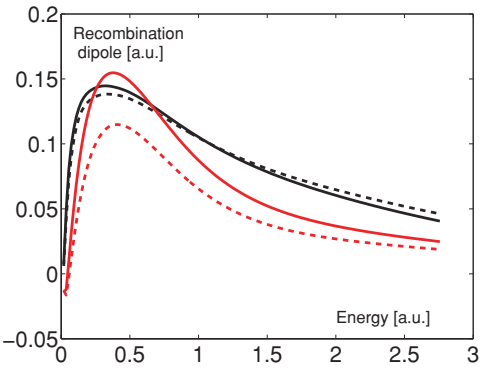

FIG. 8. (Color online) Recombination dipoles calculated with (solid line) and without (dashed line) exchange contributions. Black and red curves show the real and imaginary parts of the recombination dipole, respectively.

ionization and recombination in HHG are associated with the ground (X) and first excited (A) ionic states of N_2^+, the $X\,^2\Sigma_g$ and $A^2\Pi_u$.

The norms of both Dyson orbitals are close to unity (with total N-electron wave function normalized to N), suggesting that one-electron dipole recombination with both ionic states is possible already in the HF approximation, in contrast with the case of H_2. Thus, we expect that the contribution of the exchange term to the excited state channel will be much less significant than in the previous case.

Figure 8 shows the recombination dipole for the A channel, calculated with and without exchange contributions. We show separately the real (black) and imaginary (red) parts of the recombination dipole. Overall, the exchange contribution increases the recombination dipole, consistent with the general expression Eqs. (40) and (41) and the choice of signs of the Dyson orbitals, which uniquely determines the sign of the transition dipole between X and A states.

Calculations of the bound states used complete active space self-consistent field (CASSCF) method with correlation-consistent valence triple-ζ basis-set expansion, while the strong-field eikonal-Volkov approximation [84] was used for the continuum states. The role of the exchange contributions is significantly less than in the case of the 2-hole 1-particle state discussed earlier.

In general, the preceding analysis shows that the importance of exchange (cradle) terms can be quickly assessed by looking at the norm of the corresponding Dyson orbital. If this norm is close to unity, as is the case for both channels of interest in N_2, the direct term would likely dominate.

VI. CONCLUSION

Our analysis shows that electron exchange can significantly alter structural features in the high harmonic spectra, associated with direct photorecombination. Electron exchange during recombination can be viewed as a dipole transition that changes the electronic state of the ion, followed by the recombination of the continuum electron into the new hole. This second step is determined by the overlap of

the continuum wave packet with the Dyson orbital for the new ionic state. This overlap encodes structural properties of the new Dyson orbital, different from that for direct recombination.

In our model system, electron-electron repulsion leads to the destructive interference of direct and exchange contributions. In general, destructive interference of direct and exchange contributions to HHG may create additional minima in the harmonic spectra, unrelated to orbital structures. Further, polarization of the neutral molecule can also strongly mask structural minima and maxima.

The role of two-electron excitations in HHG has largely been underestimated so far. Our calculations show the importance of this channel, which becomes excited not by strong-field ionization, but by the returning electron prior to recombination.

The general expression Eq. (40), which associates exchange with the dipole transition in the ion, suggests that the exchange terms will likely dominate in the case of two-electron excitation (two-hole one-particle states in the HF picture). Indeed, the dipole operator acting on the ionic states can change the electronic excitation in the ion from the two-hole to one-hole configuration. The latter is naturally suited for the recombination of the continuum electron.

ACKNOWLEDGMENTS

We acknowledge support of the NSERC SRO program. M.I. acknowledges the support of the Alexander von Humboldt Foundation. S.S., O.S., and M.I. acknowledge the support of the Kavli Institute for Theoretical Physics and its "Quantum Control of Light and Matter" program.

[1] For recent reviews, see, for example, M. Lein, J. Phys. B **40**, R135 (2007); F. Krausz and M. Ivanov, Rev. Mod. Phys. **81**, 163 (2009).
[2] P. B. Corkum, Phys. Rev. Lett. **71**, 1994 (1993).
[3] S. Baker *et al.*, Science **312**, 424 (2006); Phys. Rev. Lett. **101**, 053901 (2008).
[4] S. Patchkovskii, Phys. Rev. Lett. **102**, 253602 (2009).
[5] N. Wagner *et al.*, Proc. Natl. Acad. Sci. USA **103**, 13279 (2006).
[6] W. Li *et al.*, Science **322**, 1207 (2008).
[7] M. Spanner and P. Brumer, Phys. Rev. A **78**, 033840 (2008).
[8] R. Santra and A. Gordon, Phys. Rev. Lett. **96**, 073906 (2006).
[9] S. Patchkovskii, Z. Zhao, T. Brabec, and D. M. Villeneuve, Phys. Rev. Lett. **97**, 123003 (2006).
[10] Z. Zhao, J. Yuan, and T. Brabec, Phys. Rev. A **76**, 031404 (2007).
[11] A. T. Le, R. R. Lucchese, S. Tonzani, T. Morishita, and C. D. Lin, Phys. Rev. A **80**, 013401 (2009).
[12] A. T. Le, R. R. Lucchese, and C. D. Lin, J. Phys. B **42**, 211001 (2009).
[13] S. Sukiasyan, C. McDonald, C. Destefani, M. Y. Ivanov, and T. Brabec, Phys. Rev. Lett. **102**, 223002 (2009).
[14] M. V. Frolov, N. L. Manakov, T. S. Sarantseva, M. Y. Emelin, M. Y. Ryabikin, and A. F. Starace, Phys. Rev. Lett. **102**, 243901 (2009).
[15] O. Smirnova *et al.*, Nature (London) **460**, 972 (2009).
[16] O. Smirnova *et al.*, Proc. Natl. Acad. Sci. USA **106**, 16556 (2009).
[17] O. Smirnova, S. Patchkovskii, Y. Mairesse, N. Dudovich, D. Villeneuve, P. Corkum, and M. Y. Ivanov, Phys. Rev. Lett. **102**, 063601 (2009).
[18] S. Haessler *et al.*, Nat. Phys. **6**, 200 (2010).
[19] B. K. McFarland *et al.*, Science **322**, 1232 (2008).
[20] T. Brabec, M. Cote, P. Boulanger, and L. Ramunno, Phys. Rev. Lett. **95**, 073001 (2005).
[21] S. V. Popruzhenko, V. D. Mur, V. S. Popov, and D. Bauer, Phys. Rev. Lett. **101**, 193003 (2008).
[22] A. Lühr, Y. V. Vanne, and A. Saenz, Phys. Rev. A **78**, 042510 (2008).
[23] Y. V. Vanne and A. Saenz, Phys. Rev. A **80**, 053422 (2009).
[24] Y. V. Vanne and A. Saenz, Phys. Rev. A **79**, 023421 (2009).
[25] S. Petretti *et al.*, Phys. Rev. Lett. (to be published).
[26] M. Abu-samha and L. B. Madsen, Phys. Rev. A **80**, 023401 (2009).
[27] Song-Feng Zhao, C. Jin, A. T. Le, T. F. Jiang, and C. D. Lin, Phys. Rev. A **80**, 051402 (2009).
[28] S.-F. Zhao, C. Jin, A. T. Le, T. F. Jiang, and C. D. Lin, Phys. Rev. A **81**, 033423 (2010).
[29] M. Spanner and S. Patchkovskii, Phys. Rev. A **80**, 063411 (2009).
[30] M. Kitzler, J. Zanghellini, C. Jungreuthmayer, M. Smits, A. Scrinzi, and T. Brabec, Phys. Rev. A **70**, 041401 (2004).
[31] G. Jordan *et al.*, J. Phys. B **39**, S341 (2006).
[32] Y. Mairesse *et al.*, Phys. Rev. Lett. (to be published).
[33] O. Smirnova, M. Spanner, and M. Ivanov, J. Mod. Opt. **54**, 1019 (2007).
[34] G. Jordan and A. Scrinzi, New J. Phys. **10**, 025035 (2008).
[35] M. Lezius, V. Blanchet, D. M. Rayner, D. M. Villeneuve, A. Stolow, and M. Y. Ivanov, Phys. Rev. Lett. **86**, 51 (2001).
[36] A. N. Markevitch, S. M. Smith, D. A. Romanov, H. B. Schlegel, M. Y. Ivanov, and R. J. Levis, Phys. Rev. A **68**, 011402(R) (2003).
[37] A. Gordon, F. X. Kartner, N. Rohringer, and R. Santra, Phys. Rev. Lett. **96**, 223902 (2006).
[38] J. Zanghellini, Ch. Jungreuthmayer, and T. Brabec, J. Phys. B **39**, 709 (2006).
[39] M. Ruggenthaler, S. V. Popruzhenko, and D. Bauer, Phys. Rev. A **78**, 033413 (2008).
[40] M. Yu. Ivanov, T. Brabec, and N. Burnett, Phys. Rev. A **54**, 742 (1996).
[41] M. Yu Kuchiev and V. N. Ostrovsky, J. Phys. B **34**, 405 (2001).
[42] G. L. Yudin and M. Yu. Ivanov, Phys. Rev. A **63**, 033404 (2001).
[43] P. Agostini and L. F. DiMauro, Rep. Prog. Phys. **67**, 813 (2004).
[44] P. Salières, A. L'Huillier, and M. Lewenstein, Phys. Rev. Lett. **74**, 3776 (1995).
[45] P. Salières *et al.*, Science **292**, 902 (2001).
[46] M. Yu. Kuchiev and V. N. Ostrovsky, J. Phys. B **32**, L189 (1999).
[47] M. Yu. Kuchiev and V. N. Ostrovsky, Phys. Rev. A **60**, 3111 (1999).
[48] R. Kopold, W. Becker, and M. Kleber, Opt. Commun. **179**, 39 (1999).

[49] R. Kopold, D. B. Milošević, and W. Becker, Phys. Rev. Lett. **84**, 3831 (2000).
[50] D. B. Milošević, S. Hu, and W. Becker, Phys. Rev. A **63**, 011403(R) (2000).
[51] W. Becker *et al.*, Adv. At. Mol. Opt. Phys. **48**, 35 (2002).
[52] D. B. Milošević and W. Becker, Phys. Rev. A **66**, 063417 (2002).
[53] R. Kopold, W. Becker, and D. B. Milošević, Phys. Scr. **68**, C76 (2003).
[54] D. B. Milošević, G. G. Paulus, and W. Becker, Phys. Rev. A **71**, 061404(R) (2005).
[55] D. B. Milošević, D. Bauer, and W. Becker, J. Mod. Opt. **53**, 125 (2006).
[56] C. Figueira de Morisson Faria, H. Schomerus, and W. Becker, Phys. Rev. A **66**, 043413 (2002).
[57] C. F. M. Faria and W. Becker, Laser Phys. **13**, 1196 (2003).
[58] C. Figueira de Morisson Faria, X. Liu, W. Becker, and H. Schomerus, Phys. Rev. A **69**, 021402 (2004).
[59] X. Liu and C. Figueira de Morisson Faria, Phys. Rev. Lett. **92**, 133006 (2004).
[60] C. Figueira de Morisson Faria, H. Schomerus, X. Liu, and W. Becker, Phys. Rev. A **69**, 043405 (2004).
[61] A. L'Huillier *et al.*, J. Phys. B **24**, 3315 (1991).
[62] M. B. Gaarde and K. J. Schafer, Phys. Rev. Lett. **89**, 213901 (2002).
[63] M. B. Gaarde, M. Murakami, and R. Kienberger, Phys. Rev. A **74**, 053401 (2006).
[64] O. Smirnova *et al.*, J. Phys. B **40**, F197 (2007).
[65] M. Plummer and C. J. Noble, J. Phys. B **35**, L51 (2002).
[66] K. Harumiya, H. Kono, Y. Fujimura, I. Kawata, and A. D. Bandrauk, Phys. Rev. A **66**, 043403 (2002).
[67] J. S. Parker *et al.*, J. Phys. B **33**, L239 (2000).
[68] M. Lein, N. Hay, R. Velotta, J. P. Marangos, and P. L. Knight, Phys. Rev. Lett. **88**, 183903 (2002).
[69] K. C. Kulander and B. W. Shore, Phys. Rev. Lett. **62**, 524 (1989).
[70] X. Chu and Shih I. Chu, Phys. Rev. A **64**, 063404 (2001).
[71] M. H. Beck, A.-Jäckle, G. A. Worth, and H.-D. Meyer, Phys. Rep. **324**, 1 (2000).
[72] J. Frenkel, *Wave Mechanics* (Oxford University Press, 1934).
[73] P. A. M. Dirac, Proc. Cambridge Philos. Soc. **26**, 376 (1930).
[74] J. Zanghellini, M. Kitzler, T. Brabec, and A. Scrinzi, J. Phys. B **37**, 763 (2004).
[75] E. Schmidt, Math. Ann. **63**, 433 (1906).
[76] M. H. Beck and H.-D. Meyer, Z. Phys. D **42**, 113 (1997).
[77] R. Kosloff and T. Tal-Ezer, Chem. Phys. Lett. **127**, 223 (1986).
[78] S. Sukiasyan, C. McDonald, C. VanVlack, C. Destefani, T. Fennel, M. Ivanov, and T. Brabec, Phys. Rev. A **80**, 013412 (2009).
[79] K. Burnett, V. C. Reed, and P. L. Knight, J. Phys. B **26**, 561 (1993).
[80] G. Jordan and A. Scrinzi, New J. Phys. **10**, 025035 (2008).
[81] M. Lein, N. Hay, R. Velotta, J. P. Marangos, and P. L. Knight, Phys. Rev. A **66**, 023805 (2002).
[82] S. Sukiasyan *et al.* (unpublished).
[83] R. Torres *et al.*, Phys. Rev. A (to be published).
[84] O. Smirnova, M. Spanner, and M. Ivanov, Phys. Rev. A **77**, 033407 (2008).